Received: 13 February 2019 | Revised: 5 August 2019 | Accepted: 27 August 2019

DOI: 10.4218/etrij.2019-0024

ORIGINAL ARTICLE

ETRI Journal WILEY

Design of nonlinear photonic crystal fibers with ultra-flattened zero dispersion for supercontinuum generation

Pranaw Kumar | **Kokou Firmin Fiaboe** | **Jibendu Sekhar Roy**

School of Electronics Engineering, Kalinga Institute of Industrial Technology, Bhubaneswar, Odisha, India

Correspondence
Pranaw Kumar, School of Electronics Engineering, Kalinga Institute of Industrial Technology, Odisha, India.
Email: kumarpranaw9@gmail.com

The study reports on the design and performance of two air-filled and two partial ethanol-filled photonic crystal fiber (PCF) structures with a tetra core for supercontinuum generation. The PCFs are nonlinear with ultra-flattened zero dispersion. Holes with smaller areas are used to create a tetra-core PCF structure. Ethanol is filled in the holes of smaller area while the larger holes of cladding region are air-filled. Optical properties including dispersion, effective mode area, confinement loss, normalized frequency, and nonlinear coefficient of the designed PCF structures are investigated via full vector finite difference time domain (FDTD) method. A PCF structure with lead silicate as wafer exhibits significantly better results than a PCF structure with silica as wafer. However, both structures report dispersion at a telecommunication wavelength corresponding to 1.55 μm. Furthermore, the PCF structure with lead silicate as wafer exhibits a very high nonlinear coefficient corresponding to 1375 W^{-1} km^{-1} at the same wavelength. This scheme can be used for optical communication systems and in optical devices by exploiting the principle of nonlinearity.

KEYWORDS

dispersion, nonlinear coefficient, photonic crystal fibers, supercontinuum generation

1 | INTRODUCTION

Photonic crystal fibers (PCFs) have attracted researchers since the first structure was proposed by Russell in the 1990s [1].

Many unique features including dispersion [2], birefringence [3], effective mode area [4], endless single-mode propagation [5], and high nonlinear coefficient [6] make PCFs significantly superior when compared to standard fibers. Holey fibers or microstructured optical fibers allow a unique way of light propagation [7], which is unusual in conventional fibers. Specifically, PCFs are composed of a single material with the periodic arrangement of multiple air holes with a defect at its center. The defect region acts as a solid core [8]. The periodic arrangement of air holes runs parallel to the longitudinal axis of the fiber. This type of a structure of fibers provides a platform to achieve the manipulation of photons. Based on the guiding mechanism, PCFs can correspond to index-guided PCFs [9] and photonic bandgap fiber [10].

An array of air holes in the cladding region with a solid core makes index-guiding PCFs. Air holes trap light propagating through the core region. They allow an interactive environment to the propagating light energy with gases and liquids present in the cladding holes with the transitory field. Light is guided through a low index core in photonic bandgap fibers. The total dispersion of PCF

corresponds to the submission of material dispersion and waveguide dispersion. Efforts focused on obtaining PCFs with ultra-flattered dispersion [11]. Specifically, PCFs offer a variety of geometries or PCF structures due to their flexibility in design, and this allows control over dispersion [12].

Several geometries of PCF are reported by introducing new design methods [13–16]. A few techniques used to achieve flattened dispersion curve include tailoring the diameter of air holes and varying the shape/dimension of air holes and air holes filled with different liquids and gases [17–19]. Smaller air holes in the innermost layer of the cladding region determine the overall flatness of the dispersion curve [20]. Saitoh and others reported a flattened dispersion curve for a triangular lattice PCF structure with a defected core of center air hole [21]. A square lattice PCF with a defected core of central air hole was investigated by Zhang and others and exhibited ultra-low dispersion [22]. Adjustment in the structural parameter of the PCFs resulted in zero chromatic dispersion and dispersion-shifted fibers [23,24]. Furthermore, fine control over the optical transmission of the polarized property of fiber results from using the air holes filled completely, partially, or selectively with different types of liquids and gases. Liquids including ethanol [25], water [26], liquid crystal [27], and polymers [28] are used to date. Gundu and others reported a PCF with extremely low dispersion by using some liquid in the holes of the two innermost layers [29]. Highly nonlinear PCFs can be used for four wave mixing and self-phase modulation (SPM). Furthermore, SPM significantly affects the dispersion behavior in a high data rate transfer system. The effective mode area is inversely proportional to the filling factor of PCFs. Liao and others reported an ultra-high nonlinear coefficient corresponding to 3.573×10^4 W^{-1} km^{-1} at 1.55 μm [30]. Hossain and others [31] introduced an elliptical air hole at the core and decreased the sizes of inner air holes to obtain a nonlinear coefficient corresponding to 83 W^{-1} km^{-1}. Hence, an octagonal PCF structure with two air holes exhibiting elliptical geometry in the inner cladding region was obtained. Wang and others reported a nonlinear coefficient of 10^{-2} m^{-1} W^{-1} with two zero dispersion points [32]. Tiwari and others [33] and R. Kumari and others [34] also reported effective nonlinear coefficients corresponding to 500 W^{-1} km^{-1} and 1179 W^{-1} km^{-1}, respectively. Single-mode PCF is required for the transmission of signals for larger distances without interference [35]. Furthermore, several geometries of PCF are examined with significantly higher nonlinearity [36–40]. Leaky nature of the modes and imperfect structure of PCF together cause confinement loss. These types of losses are reduced by the increasing number of air holes in the cladding region. Researchers reported extremely low confinement loss via modifying the PCF structure [41].

Supercontinuum generation has attracted research attention due to its wide application in the field of optics fluorescence microscopy [42], mid-infrared SCG [43,44] optical communication-based DWDM [45,46], and other application. Various efforts using several techniques focused on broadening the generated spectrum. In order to obtain the desired supercontinuum, dispersion engineering of PCFs compose of silica is performed by tailoring the physical parameters [47–49]. Furthermore, the implementation of the optofluidic approach is also adapted to widen the supercontinuum spectrum. Experimental techniques for fully or partially filling of holes in PCF are well-developed [50,51].

In the study, a tetra-core PCF structure with hexagonal lattice is investigated. PCF structure is fabricated such that a tetra core is created. Two materials, namely silica and lead silicate, are used as background materials. Two types of holes are used. Smaller holes of the cladding region are filled with ethanol. This type of a structure is investigated to achieve zero dispersion with a large nonlinear coefficient. Both structures exhibit almost zero dispersion over a wide range of wavelength with extremely low loss. Furthermore, a large nonlinear coefficient is also reported. Both structures allow single-mode propagation. Supercontinuum generation is proposed as a key technology for an application such as spectroscopy, gas detection, molecular fingerprinting, and chemical sensing. The rod filling technique is used to obtain a wide spectrum.

2 | DESIGN OF PROPOSED PCF STRUCTURES

Researchers investigated several PCF structures based on the geometry of its core. Extant studies investigated PCF structure with dual core [52], rectangular core [53], square core [54], circular core [55], Octagonal core [56], T-shaped core [57], and P-shaped core [58]. Even a quad-core PCF structure was recently examined [59]. In the study, the concept of tetra core is introduced with a new modified geometry. Furthermore, it is doped with alcoholic material. Tetra-core PCF structure with hexagonal lattice and also doped with ethanol are examined. Holes with two different dimensions (ie, smaller and larger) are used. The smaller circular hole is introduced at the center to create a quad-core PCF structure. Furthermore, the smaller holes are occasionally filled with air and ethanol. Alternate holes of all the rings are smaller in size. A description of the structures is given in Table 1.

Lead silicate is a nonlinear compound with large nonlinearity. Hence, it is used in the study to obtain PCF with a significantly higher nonlinear coefficient. Furthermore, this is used as a background material of fiber and ethanol is doped in holes of much smaller dimensions when compared to larger air circular holes. Thus, its toxic nature does not affect ethanol.

TABLE 1 Description of designed PCF structures

PCF structures	Descriptions
Silica_air	Smaller and larger circular holes of the cladding region are filled with air. It includes silica as the wafer.
Silica_Ethanol	All smaller circular holes are filled with ethanol and all larger holes are filled with air. It includes silica as the wafer.
Lead silicate_Air	Smaller and larger circular holes of the cladding region are filled with air. It includes lead silicate as the wafer.
Lead silicate_Ethanol	All smaller circular holes are filled with ethanol and all larger holes are filled with air. It includes lead silicate as the wafer.

The finite difference time domain (FDTD) method is based on a general approach and used to describe any arbitrary structure beyond its design complexity. Hence, the FDTD method is the most used technique for solving electromagnetic problems. Vectorial wave equation is given below and is derived from Maxwell's equation [60,61]

$$\nabla\times([\mathbf{S}]^{-1}\nabla\times E)-K_o n^2[\mathbf{S}]E=0 \tag{1}$$

where [**S**] denotes the 3 × 3 PML matrix and $[\mathbf{S}]^{-1}$ denotes the inverse of [**S**].

E denotes the electric field vector and "n" and "λ" denote the refractive index and operating wavelength, respectively. K_o denotes the wave number intra space and is equal to $2\pi/\lambda$. Given the speed of light in vacuum as the radiation propagation speed, the time step allowed for stable computation is estimated as follows [61]:

$$c\Delta t\le\left(\frac{1}{(\Delta x)^2}+\frac{1}{(\Delta y)^2}+\frac{1}{(\Delta z)^2}\right)^{-1/2}. \tag{2}$$

Dispersion is the change in pulse width per unit distance of propagation that separates a wave into its spectral components. Dispersion significantly affects the bit rate and bandwidth of a fiber. Control over dispersion must be achieved to ensure the feasibility of a practical application of PCFs. Dispersion of PCFs is the sum of wavelength dispersion (D_w) and material dispersion (D_m) as follows [62]:

$$D=D_w+D_m \tag{3}$$

and

$$D_m=-\frac{\lambda}{c}\frac{d^2n_m}{d\lambda^2} \tag{4}$$

where n_m denotes the refractive index of the material and is derived using Sellemier's equation [62,63]:

$$D_w=-\frac{\lambda}{c}\frac{d^2\mathrm{Re}[n_{eff}]}{d\lambda^2} \tag{5}$$

where $\mathrm{Re}[n_{eff}]$ denotes the real part of effective refractive index of the fundamental mode, and λ and c denote the operating wavelength and velocity of light in vacuum, respectively.

Mode fields spread more from the core region to the cladding region due to the low refractive index difference between the core and cladding. The imaginary part of the effective refractive index of the mode is obtained using a perfectly matched boundary condition. This imaginary part $\{\mathrm{Im}[n_{eff}]\}$ gives the calculation of mode confinement loss as follows [63]:

$$C_L=\frac{20}{\ln(10)}\times\frac{2\pi}{\lambda}\times\{\mathrm{Im}[n_{eff}]\}. \tag{6}$$

Confinement loss is expressed in dB/km.

The effective mode area represents the quantitative measurement of tightly confined mode inside the core area. The effective mode area is calculated as follows [64]:

$$A_{eff}=\frac{\left[\iint|E(x,y)dxdy|^2\right]^2}{\iint|E(x,y)dxdy|^4}. \tag{7}$$

E denotes the amplitude of a transverse electric field propagating through fiber.

Lower nonlinearity is observed by PCF with a highly effective mode area. Lower effective mode area generates high power intensity. Effective nonlinearity of PCF is obtained as follows [64]:

$$y(\lambda)=\left(\frac{2\pi}{\lambda}\right)\left(\frac{n_2}{A_{eff}}\right) \tag{8}$$

where $y(\lambda)$ = nonlinearity of PCF is measured in $\mathrm{W^{-1}\,km^{-1}}$.

λ and A_{eff} denote the operating wavelength and effective mode area of PCF at operating wavelengths, respectively, and n_2 denotes the nonlinear coefficient of the material used. Specifically, $n_2 = 3.01\times10^{-20}$ $\mathrm{m^2/W}$ for silica and $n_2 = 4.1\times10^{-19}$ $\mathrm{m^2/W}$ for lead silicate.

It should be ensured that the designed PCF operates in single-mode propagation. Hence, normalized frequency or V_{eff} is calculated as follows [64]:

$$V_{eff}=\frac{2\pi\Lambda}{\lambda}\sqrt{n_{co}^2-n_{eff}^2} \tag{9}$$

where n_{eff} and n_{co} denote the effective refractive index and refractive index of core, respectively, and λ and Λ denote the operating wavelengths and pitch factors, respectively.

An optical pulse and its evolution with slow varying electric field amplitude are represented by its envelope function $A(z, t)$ that is defined by the generalized nonlinear Schrodinger equation as follows [65,66]:

$$\frac{\partial A}{\partial Z}+\frac{\alpha}{2}A+\sum_{n\geq 2}^{n} i^{n+1}\frac{\beta_n}{n!}\frac{\partial^n A}{\partial t^n} = i\left(\gamma(\omega_0)+i\gamma_1\frac{\partial}{\partial t}\right).A(z,t)\int_{-\infty}^{t} R(t')|A(z,t-t')|^2 dt'. \quad (10)$$

The total fiber loss observed is represented by α. Specifically, Z and t denote the special coordinate along the fiber length and the time variable, γ denotes the nonlinear parameter, and β_n denotes the nth order dispersion (from second to ninth order dispersion are considered in this work). Additionally, $R(t)$ denotes response function including Raman and Kerr nonlinearity. The electronic contribution of the nearly instantaneous functional form of $R(t)$ is as follows:

$$R(t)=(1-f_R)\delta(t)+f_R h_R(t) \quad (11)$$

where f_R denotes the fractional contribution of the delay Raman response function $h_R(t)$. Furthermore, $h_R(t)$ is approximately analyzed as follows:

$$h_R(t)=\frac{\tau_1^2+\tau_2^2}{\tau_1\tau_2^2}\exp\left(\frac{t}{\tau_2}\right)\sin\left(\frac{-t}{\tau_1}\right), \quad (12)$$

where $f_R = 0.18$, $\tau_1 = 12.2$ fs, and $\tau_2 = 32$ fs.

The Dirac delta function is denoted as $\delta(t)$.

3 | SIMULATIONS AND RESULTS

A four tetra-core PCF structure is simulated using the FDTD method. Silica and lead silicate are used as background materials. The simulated PCF structure consists of 11 rings of circular holes in the cladding region. Two types of holes are used to design the simulated PCF structure. Smaller holes are used to create a tetra-core PCF structure. The schematic diagram and refractive index distribution of the proposed structure are shown in Figures 1 and 2. Furthermore, alternate rings exhibit smaller holes in the cladding structure. All the smaller holes are filled with ethanol. Pitch factor and hole-to-hole spacing considered for the proposed structure correspond to 1 μm. Smaller holes exhibit a diameter corresponding to 0.4 μm. The radius of larger air holes corresponds to 1.2 μm. The PML thickness is considered as 10%. The thickness is based on several previously reported and already cited research papers [67]. Fabrication of PCF is performed via different techniques due to the changes in the refractive index during fabrication [68,69]. Large air-filling fraction in the cladding region aids in achieving tight confinement into a small core. This results in higher order waveguide that can even cancel large negative dispersion of silica glasses [70]. Further PCF doped with different materials were also produced and fabricated [71,72].

Chromatic dispersion causes a change in the optical pulse per unit distance of the propagating length of fibers. Both the simulated PCF structures report flattened dispersion at all the four optical windows. The PCF structure with silica as wafer displays extremely low dispersion. The reported value is even less than 5 ps/(nm-km). Furthermore, zero dispersion is reported at the telecommunication wavelength of 1.55 μm. However, PCF structure with lead silicate as wafer exhibits nearly zero dispersion at all the four optical windows. These types of dispersion values make the stimulated PCFs structure applicable in high data rate transmission. Figure 3 shows the dispersion as a function of wavelength.

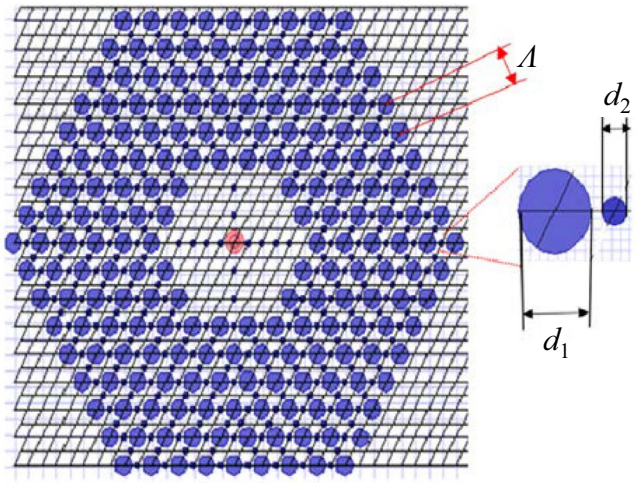

FIGURE 1 Proposed PCF structure

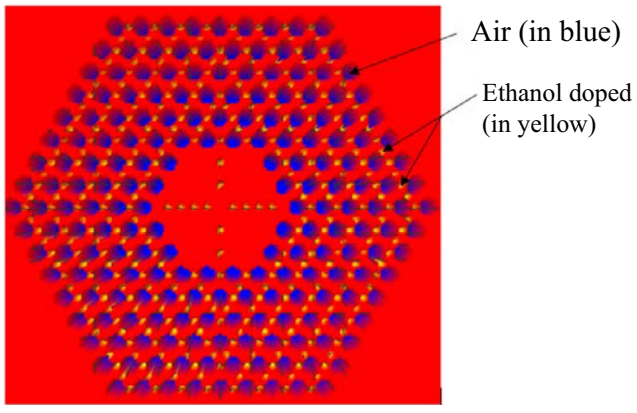

FIGURE 2 Refractive index distribution of the proposed PCF structure

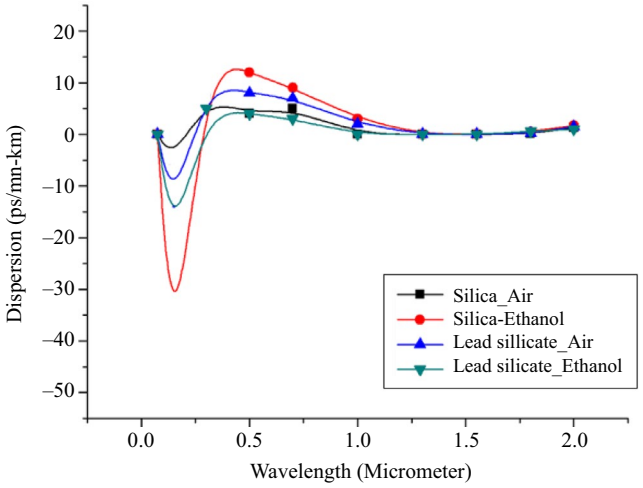

FIGURE 3 Dispersion behavior

A small portion of energy leaks out of incident radiation from the core to the cladding region during its propagation through fibers. This is termed as leaky loss or confinement loss. An increase in the size of the holes of the cladding region decreases the width of the silica bridge that is formed between adjacent holes. This leads to a decrease in leakage loss. The obtained confinement loss at different operating wavelengths is plotted in Figure 4. The PCF with silica as the wafer reports higher confinement loss when compared with the other PCF structure with lead silicate as a wafer. However, both the PCF structures exhibit ultra-low confinement loss. The observed magnitude of the confinement loss is of the order 10^{-8}.

Leakage of modes through holes present in the cladding region occurs through bridges formed in between the holes. It increases the effective area of mode propagating through fibers. Figure 5 shows the effective mode area of the simulated PCF structure as a function of wavelength. The PCF structure with silica exhibits a higher effective mode area than the PCF structure with lead silicate as a wafer. However, the effective mode

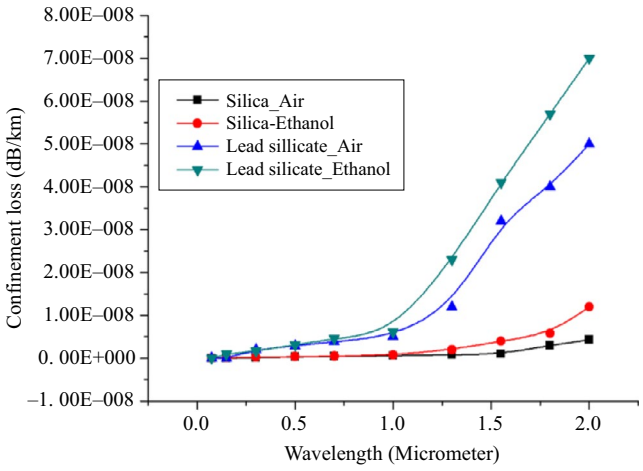

FIGURE 4 Confinement loss behavior

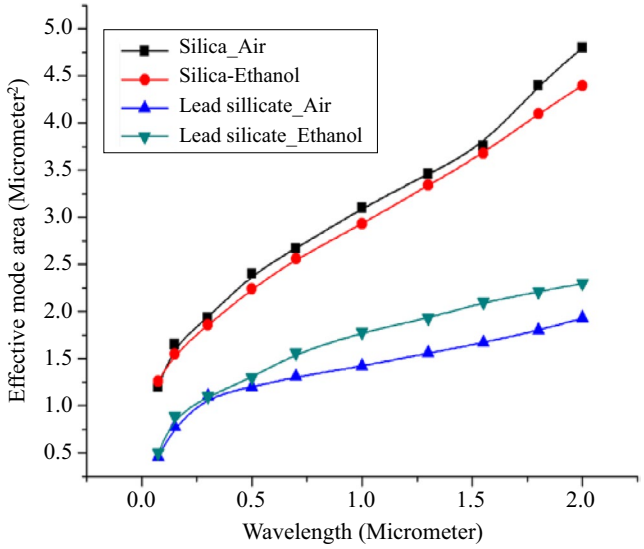

FIGURE 5 Effective mode area

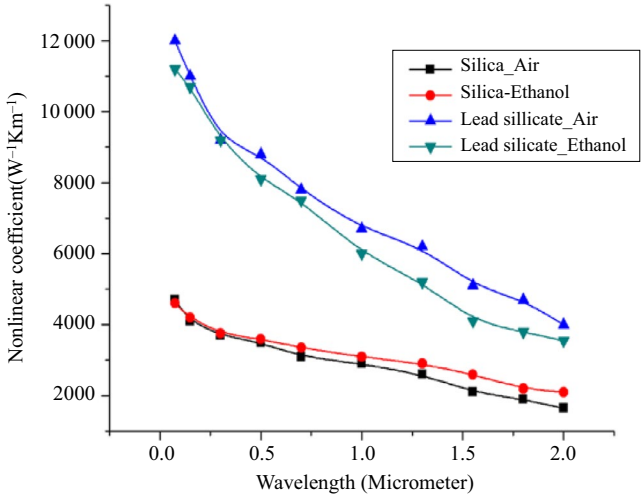

FIGURE 6 Effective nonlinearity

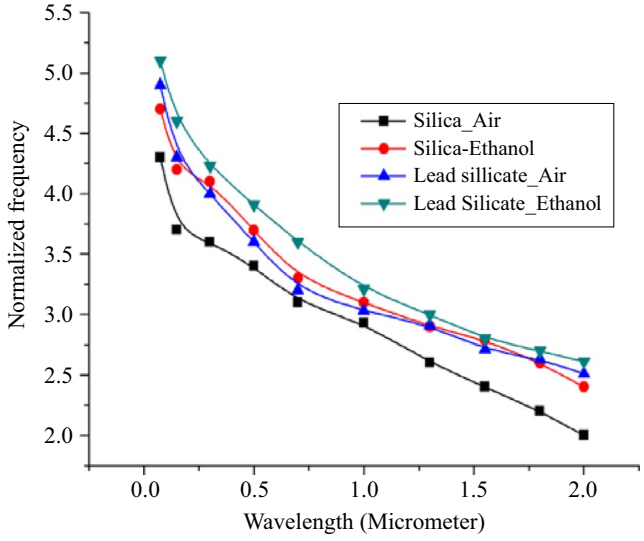

FIGURE 7 Normalized frequency

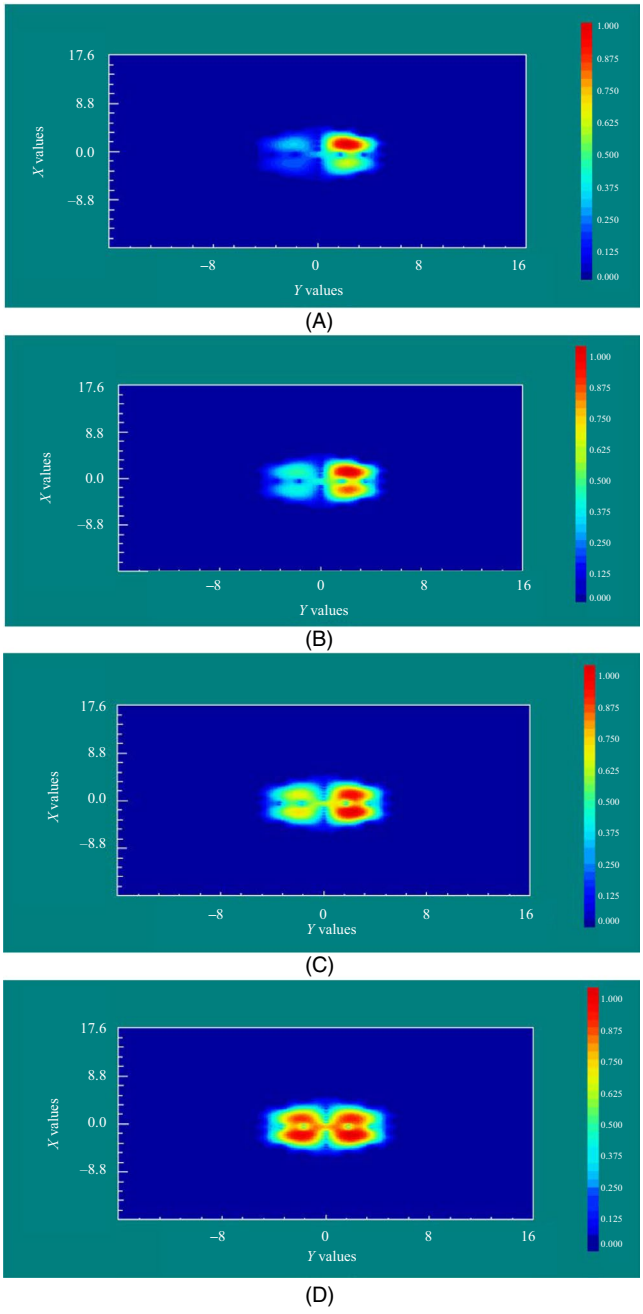

FIGURE 8 Mode confinement at (A) 0.3 μm, (B) 0.7 μm, (C) 0.85 μm, and (D) 1.55 μm

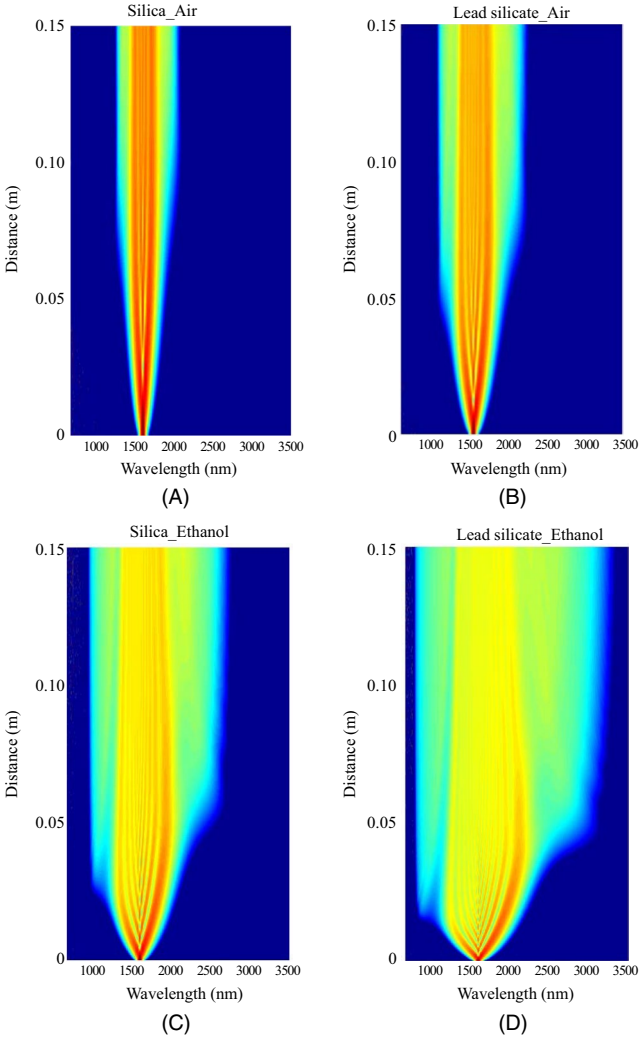

FIGURE 9 Spectral profile of a 15-cm length of PCF with (A) Silica_Air, (B) Lead silicate_Air, (C) Silica_Ethanol, and (D) Lead Silicate_Ethanol

area increases with increases in the wavelength. As previously stated, the effective mode area is inversely proportional to the nonlinear coefficient. The PCF structure with lead silicate as wafer exhibits a higher nonlinear coefficient than that of the PCF structure with silica as a wafer. At the communication

TABLE 2 Values of dispersion order at a wavelength of 1.55 μm

$\beta_n(ps^n/m)$	Silica_Air	Lead silicate _Air	Silica_Ethanol	Lead silicate_Ethanol
β_2	5.48	2.95	8.76	7.54
β_3	-4.59×10^{-3}	-1.15×10^{-3}	-3.96×10^{-3}	-2.89×10^{-3}
β_4	1.56×10^{-5}	9.02×10^{-6}	5.93×10^{-6}	6.83×10^{-6}
β_5	-8.45×10^{-9}	-2.47×10^{-9}	-5.64×10^{-9}	-1.67×10^{-9}
β_6	4.58×10^{-12}	4.24×10^{-12}	1.52×10^{-12}	2.76×10^{-12}
β_7	-7.95×10^{-15}	-6.43×10^{-15}	-3.28×10^{-15}	-4.47×10^{-15}
β_8	3.46×10^{-18}	3.35×10^{-17}	7.48×10^{-18}	8.64×10^{-17}
β_9	-7.78×10^{-21}	-8.45×10^{-20}	8.90×10^{-21}	-3.85×10^{-20}

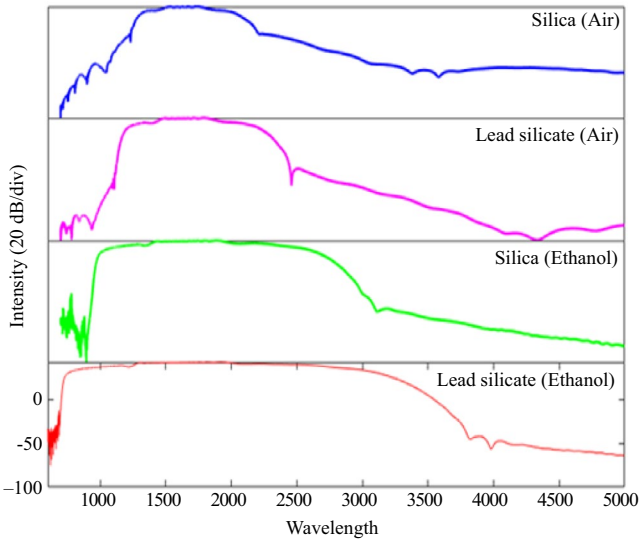

FIGURE 10 Supercontinuum coherence at the output of the fiber for the Silica_Air, Lead silicate_Air, Silica_Ethanol, and Lead silicate_Ethanol when pumped at 1550 nm

TABLE 3 Comparison of supercontinuum bandwidth (in nm) measured at –40 dB at a wavelength of 1550 nm of a 15-cm length fiber for all the examined PCF structures

Silica_air	Lead silicate _Air	Silica_Ethanol	Lead silicate _Ethanol
631 nm	1045 nm	1973 nm	2784 nm

wavelength, the PCF structure with lead silicate exhibits an effective nonlinearity corresponding to 6200 W^{-1} km^{-1}. Figure 6 shows the relation between obtained effective nonlinearity at different operating wavelength.

Normalized frequency is typically termed as V_{eff} and ensures single-mode property of fibers. A standard fiber with V-parameter ≤2.405 assures single-mode propagation. With respect to PCF, V_{eff} ≤4.1 assures endless single-mode propagation. Figure 7 shows the plot for V_{eff} at corresponding wavelengths. The magnitude of $V_{eff,}$ as obtained from Figure 7 confirms that the designed PCF supports endless single-mode propagation.

Figure 8 shows the mode field confinement at the telecommunication wavelength. As shown in the figure, the effective area of the optical field is tightly confined at tetra-core PCF. It also shows the strong confinement of mode or mode field distribution within the core. Figure 8A represents the confinement of mode at a lower wavelength (0.3 μm). In Figure 8B, confinement of mode is introduced in the second core at 0.7 μm. Similarly, at the wavelength of 0.85 μm, modes get more confined in two cores. Confinement of the mode in all four cores appears at a higher wavelength as shown in Figure 8C and 8D.

Figure 9 shows the capability of the liquid infiltration technique for supercontinuum generation with flattened bandwidth. It is achieved by simply selecting an appropriate liquid and also exhibits excessive coherence because β_4 (fourth-order dispersion) is positive. Hence, we select ethanol as our desired infiltrating liquid for optical coherence tomography and other supercontinuum generation applications.

Supercontinuum generation is discussed with each of the PCFs examined in the study with a length corresponding to 15 cm. All the examined PCFs reported zero dispersion at a wavelength of 1.55 μm. Other values of different higher order terms of dispersion are listed in Table 2. An optical pulse of duration corresponding to 50 fs at 1550 nm is used for supercontinuum generation. Numerical simulation for supercontinuum generation is performed for all the four PCFs structure at a peak power of 5 kW. Figure 9A shows the spectral evolution of the input pulse over the entire 15 cm length of the fiber. Spectral broadening is initially

TABLE 4 Comparison of different values of dispersion and nonlinearity for previously reported PCF structure at the wavelength corresponding to 1.55 μm

References	Disper-sion (ps/nm.km)	Nonli-nearity ($w^{-1}Km^{-1)}$	Confine-ment loss (dB/km)	Effective mode area (μm^2)
[2] in (2017)	–120	14	10^{-4}	340
[37] in (2018)	N/A	3×10^4	N/A	7.8
[38] in (2019)	–110	7.8×10^4	N/A	N/A
[45] in (2012)	–199	83	N/A -	- N/A
[47] in (2011)	32	500	10^{-6}	7
[48] in (2003)	41	1179	10^2	7.1
[73] in (2013)	–15	111.5	10^3	18
[74] in (2018)	30	50	N/A	4.3
[75] in (2015)	50	300	N/A	0.7
[76] in (2017)	100	50	10^2	4.3
[77] in (2019)	–90	4200	N/A	N/A
Proposed work	0	6200	10^{-8}	4.8

observed due to self-phase modulation. Subsequently, a broader spectrum is created due to higher order nonlinearity like Raman scattering and four-wave mixing. The spectrum obtained at the end of 15 cm exhibits a width of 631 nm. Similarly, the process is repeated for the remaining PCFs structures, and the result is plotted in Figure 9B-D. Supercontinuum coherence at the output of the fiber for the PCF structure with Silica_Air, Lead silicate_Air, Silica_Ethanol, and Lead silicate_Ethanol pumped at 1550 nm is shown in Figure 10. The supercontinuum spectra obtained for the peak power of 5 kW for the PCF structure with Silica_Air, Lead silicate_Air, Silica_Ethanol, and Lead silicate_Ethanol correspond to 631 nm, 1045 nm, 1973 nm, and 2784 nm, respectively.

Comparison of Supercontinuum bandwidth (in nm) measured at the operating wavelength of 1550 nm of a fiber length of 15 cm is tabulated in Table 3.

Comparison of dispersion and nonlinearity of previously reported PCF structures at an operating wavelength of 1.55 μm is tabulated in Table 4.

4 | CONCLUSION

In the study, four PCF structures with ethanol filled holes were investigated. Silica and lead silicate were used as the background materials for the two structures. The hole with the smaller area was filled with ethanol. Holes of the cladding region were air filled. The PCF structure with lead silicate as wafer displayed flattened zero dispersion and ultra-low loss at telecommunication wavelength. Furthermore, the structure exhibited a very high nonlinearity of 6200 W^{-1} km^{-1} at 1.55 μm. However, the PCF structure with silica as wafer also indicated extremely low dispersion over a wide range of wavelengths. It also reported zero dispersion at 1.55 μm and extremely low confinement loss. Thus, both the simulated structures exhibited good results and were observed as applicable in both linear and nonlinear applications. Numerical simulation for supercontinuum generation was performed for all the PCF structures. The supercontinuum spectra for a peak power of 5 kW was 2784 nm.

ORCID

Pranaw Kumar https://orcid.org/0000-0002-6078-6258
Kokou Firmin Fiaboe https://orcid.org/0000-0001-9540-0872

REFERENCES

1. J. C. Knight et al., *All-silica single-mode optical fiber with photonic crystal cladding*, Opt. Lett. **21** (1996), 1547–1549.
2. P. Kumar et al., *Dodecagonal photonic crystal fibers with negative dispersion and low confinement loss*, Optik **144** (2017), 363–369.
3. O. Blanch et al., *Highly birefringent photonic crystal fibres*, Opt. Lett. **25** (2000), 1325–1327.
4. X. Freng et al., *Single-mode tellurite glass holey fibre with extremely large mode area for infrared nonlinear applications*, Opt. Express **16** (2008), no. 18, 13651–13656.
5. T. A. Birks, J. C. Knight, and P. S. Russell, *Endlessly single-mode photonic crystal fiber*, Opt. Lett. **22** (1997), 961–963.
6. S. M. A. Razza and Y. Namihira, *Proposal for highly nonlinear dispersion-flattened octagonal photonic crystal fibers*, IEEE Photon. Technol. Lett. **20** (2008), 249–251.
7. J. C. Knight and J. Russell, *Applied optics: New ways to guide light*, Sci. **296** (2002), 276–277.
8. A. Medjouri et al., *Design of a circular photonic crystal fiber with flattened chromatic dispersion using a defected core and selectively reduced air holes: Application to supercontinuum generation at 1.55μm*, Photon. Nanostruc. Funda. Appl. **16** (2015), 43–50.
9. J. Wang et al., *Properties of index guided PCF with air core*, Opt. Laser Tech. **39** (2006), 317–321.
10. J. C. Knight et al., *Photonic band gap guidance in optical fibers*, Sci. **282** (1998), 1476–1478.
11. W. H. Reeves et al., *Demonstration of ultra-flattened dispersion in photonic crystal fibers*, Opt. Express **10** (2002), 609–613.
12. P. J. Roberts et al., *Control of dispersion in photonic crystal fiber*, J. Opt. Fiber. Commun. Rep. **2** (2005), 435–461.
13. Y. S. Lee et al., *Diamond unit cell photonic crystal fiber with high birefringence and low confinement loss based on circular air holes*, Appl. Opt. **54** (2015), no. 20, 6140–6145.
14. Y. Ni et al., *Dual-core photonic crystal fiber for dispersion compensation*, IEEE Photon. Technol. Lett. **16** (2004), 1516–1518.
15. S. K. Biswas et al., *A modified design of a hexagonal circular photonic crystal fiber with large negative dispersion properties and ultrahigh birefringence for optical broadband communication*, Photon. **6** (2019), 1–14.
16. S. Biswas et al., *Design of an ultrahigh birefringence photonic crystal fiber with large nonlinearity using all circular air holes for a fiber-optic transmission system*, Photon. **5** (2018), 1–11.
17. G. Stepniewski et al., *Broadband supercontinuum generation in normal dispersion all-solid photonic crystal fiber pumped near 1300 nm*, Laser Phy. Lett. **11** (2017), no. 5, article no. 55103.
18. L. Cherbi et al., *Modelling of two rings photonic crystal fiber with scalar element method*, J. Optoelectron. Adv. Mater. **15** (2013), no. 11–12, 1385–1391.
19. F. Poletti et al., *Inverse design and fabrication tolerances of ultra-flattened dispersion holey fibers*, Opt. Express **13** (2005), 3728–3736.
20. K. Saitoh, N. Florous, and M. Koshiba, *Ultra flattened chromatic dispersion controllability using a defected-core photonic crystal fiber with low confinement loss*, Opt. Express **13** (2005), 8365–8371.
21. M. Zhang et al., *Dispersion ultra-flattened square lattice photonic crystal fiber with small effective mode area and low confinement loss*, Optik **125** (2014), 1610–1614.
22. Z. L. Liu et al., *Characteristics of a large negative dispersion and low confinement losses PCF*, Semicond. Optoelectr, (2008).
23. K. Saitoh et al., *Chromatic dispersion control in photonic crystal fibers: application to ultra-flattened dispersion*, Opt. Express **11** (2003), 843–852.
24. T. L. Wu and C. H. Chao, *A novel ultra-flattened dispersion photonic crystal fiber*, IEEE Photon. Technol. Lett. **17** (2005), 67–69.
25. S. Yiou, *Simulated Raman scattering in an ethanol core microstructured optical fiber*, Opt. Express **13** (2005), 4786–4791.
26. C. Martelli et al., *Water core fresnel fiber*, Opt. Express **13** (2005), 3890–3895.
27. T. T. Alkeskjod, *Highly tunable large core single mode liquid crystal photonic band gap fiber*, App. Opt. **45** (2006), 2261–2264.

28. F. M. Cox, A. Agyorus, and M. C. J. Large, *Liquid filled hollow core microstructured polymer optical fiber*, Opt. Express **14** (2006), 4135–4140.
29. K. M. Gundu, M. Kolesik, and J. V. Moloney, *Ultra-flattened-dispersion selectively liquid-filled photonic crystal fiber*, Opt. Express **14** (2006), 6870–6878.
30. J. Liao and T. Huang, *Highly nonlinear photonic crystal fiber with ultrahigh birefringence using a nano-scale slot core*, Opt. Fiber Technol. **22** (2015), 107–112.
31. M. A. Hossain, Y. Namihira, and M. A. Islam, *Polarization maintaining highly nonlinear photonic crystal fiber for supercontinuum generation at 1.55μm*, Opt. Laser Technol. **44** (2012), 1261–1269.
32. W. Wang et al., *Characteristics analysis of high birefringence and two zero dispersion points photonic crystal fiber with octagonal lattices*, Acta Phy. Sin. **61** (2012), 144601–144607.
33. M. Tiwari and V. Janyani, *Two octave spanning supercontinuum in a soft glass photonic crystal fiber suitable for 1.55-μm pumping*, J. Lightwave Technol. **29** (2011), no. 23, 3560–3565.
34. R. Kumari, M. Sharma, and S. Konar, *Lead silicate fiber with small dispersion and large nonlinearity at telecommunication wavelength*, Optik **126** (2015), 2659–2662.
35. J. S. Chiang and T. L. Wu, *Analysis of propagation characteristics for an octagonal photonic crystal fiber (O-PCF)*, Opt. Commun. **258** (2006), 170–176.
36. N. J. Flororus, K. Saitoh, and M. Koshiba, *The role of artificial defects for engineering large effective mode area, flat chromatic dispersion and low leakage losses in photonic crystal fibers: towards high speed reconfigurable transmission platforms*, Opt. Express **14** (2006), 901–913.
37. B. K. Paul et al., *Nanoscale GaP strips based photonic crystal fiber with high nonlinearity and high numerical aperture for laser applications*, Results Phys. **10** (2018), 374–378.
38. Y. E. Monfared et al., *Selectively toluene-filled photonic crystal fiber Sagnac interferometer for temperature sensing applications*, Results Phys. **13** (2019), 1–6.
39. Y. E. Monfared and S. A. Ponomarenko, *Highly nonlinear liquid-filled photonic crystal fibers*, in Proc. Photon, North (PN), Ottawa, Canada, June, 2015, p. 1.
40. Y. E. Monfared and S. A. Ponomarenko, *Slow light generation in liquid-filled photonic crystal fibers via stimulated Brillouin scattering*, Optik. Int. J. Light Electron Opt. **127** (2016), 5800–5805.
41. H. Ademgil and S. Haxha, *Highly birefringent photonic crystal fibers with ultralow chromatic dispersion and low confinement losses*, J. Lightwave Techonol. **26** (2008), 441–448.
42. Y. Sun et al., *Characterization of an orange acceptor fluorescent protein for sensitized spectral fluorescence resonance energy transfer microscopy using a white light laser*, J. Biomed. Opt. **14** (2009), 054009–054011.
43. H. Saghaei et al., *Ultra-wide mid-infrared supercontinuum generation in As40Se60 chalcogenide fibers: solid core PCF versus SIF, selected topics in quantum electronics*, IEEE J. **22** (2016), no. 2, 1–8.
44. H. Saghaei, M. Ebnali-Heidari, and M. K. Moravvej-Farshi, *Midinfrared supercontinuum generation via As_2 Se_3 chalcogenide photonic crystal fibers*, Appl. Opt. **54** (2015), no. 8, 2072–2079.
45. A. Marandi et al., *Mid-infrared supercontinuum generation in tapered chalcogenide fiber for producing octave-spanning frequency comb around 3 μm*, Opt. Express **20** (2012), no. 22, 24218–24225.
46. H. Saghaei et al., *Novel approach to adjust the step size for closed-loop power control in wireless cellular code division multiple access systems under flat fading*, IET Commun. **5** (2011), no. 11, 1469–1483.
47. F. Begum et al., *Supercontinuum generation in square photonic crystal fiber with nearly zero ultra-flattened chromatic dispersion and fabrication tolerance analysis*, Opt. Commun. **284** (2011), no. 4, 965–970.
48. K. Saitoh et al., *Chromatic dispersion control in photonic crystal fibers: application to ultra-flattened dispersion*, Opt. Express **11** (2003), no. 8, 843–852.
49. W. J. Wadsworth et al., *Supercontinuum generation in photonic crystal fibers and optical fiber tapers: a novel light source*, JOSA B **19** (2002), no. 9, 2148–2155.
50. S. Wang et al., *Selective filling of photonic crystal fibers using focused ion beam milled microchannels*, Opt. Express **19** (2011), no. 18, 17585–17590.
51. K. Nielsen et al., *Selective filling of photonic crystal fibres*, J. Opt. A Pure Appl. Opt. **7** (2005), no. 8, L:13–L:20.
52. Y. Ni et al., *Dual-core photonic crystal fiber for dispersion compensation*, IEEE Photon. Technol. Lett. **16** (2004), 1516–1518.
53. T. S. Reena et al., *Rectangular-core large mode area photonic crystal fiber for high power applications: Design and analysis*, Appl. Opt. **55** (2016), 4095–4100.
54. M. S. Islam et al., *A novel approach for spectroscopic chemical identification using photonic crystal fiber in the terahertz regime*, IEEE Sens. J. **18** (2018), 575–582.
55. S. Rana et al., *Single mode porous fiber for low loss polarization maintaining terahertz transmission*, Opt. Eng. **55** (2016), 1–6.
56. C. S. Kumar and R. Anbazhagan, *Investigation on chalcogenide and silica based photonic crystal fibers with circular and octagonal core, AEU – Int*, J. Electron. Commun. **72** (2017), 40–45.
57. P. Kumar, A. Tripathy, and J. S. Roy, *Design and analysis of single mode photonic crystal fibers with zero dispersion and ultra-low loss*, Int. J. Electron. Telecommun. **64** (2018), no. 4, 541–546.
58. P. S. Majhi and R. Choudhary, *Circular photonic crystal fibers: numerical analysis of chromatic dispersion and loss*, ISRN Opt. **2013** (2013), 1–9.
59. P. Kumar, V. Kumar, and J. S. Roy, *Design of quad core photonic crystal fibers with flattened zero dispersion*, Int. J. Electron. Commun. (AEÜ) **98** (2019), 265–272.
60. F. Zolla et al., Foundations of photonic crystal fibers. Published by Imperial College Press and distributed by World Scientific Publishing Co., 2005.
61. A. Ghatak and K. Thyagarajan, Introduction to Fiber Optics, 1st, ed, South Asian Edition, 1999.
62. J. D. Joannopoulos et al., Photonic Crystal Fiber: Molding the Flow of Light, 2nd ed, Princeton University Press, Princeton, NJ, 2008.
63. K. Thyagarajan et al., *A novel design of a dispersion compensating fiber*, IEEE photon. Technol. Lett. **8** (1996), 1510–1512.
64. G. Agrawal, Nonlinear Fiber Optics, 2nd ed, Academic Press, New York, NY, 1995.
65. J. M. Dudely and J. R. Tylor, Supercontinuum generation in optical fibers, Cambridge University Press, Cambridge, UK, 2010.
66. P. Kumar, K. F. Fiaboe, and J. S. Roy, *Highly birefringent do-octagonal photonic crystal fibers with ultra-flattened zero dispersion for supercontinuum generation*, J. Microwaves, Optoelectron. Electromagn. Applicat. **18** (2019), no. 1, 80–95.
67. M. S. Islam et al., *Porous core photonic crystal for ultra-low material loss in terahertz regime*, IET Commun. **10** (2018), no. 16, 1–5.
68. T. M. Monmor et al., *Modelling large air fraction holey optical fibers*, J. Lightwave Technol. **18** (2000), 50–54.

69. N. M. Dragomir et al., *Refractive index profiling of optical fibers using differential interference contrast microscopy*, IEEE Photon. Technol. Lett. **17** (2005), 2149–2151.
70. B. Zsigri, J. Laegsgaard, and A. Bjarklev, *A novel photonic crystal fiber design for dispersion compensation*, J. Opt. A: Pure Appl. Opt. **6** (2004), 717.
71. A. Cucinotta et al., *Amplification properties of Er3+-doped photonic crystal fibers*, J Lightwave Technol. **21** (2003), 782–788.
72. J. Fu et al., *Experimental study on all Yb-doped photonic crystal fiber laser*, in Proc. SPIE, Fiber Lasers XIV: Technol. Syst. San Francisco, CA, USA, 2017, 100832H:1–8.
73. Z. Xing-Ping et al., *High stability supercontinuum generation in lead silicate SF57 photonic crystal fibers*, Chin. Phys. B **22** (2013), 1–4.
74. M. L. Ferhat, L. Cherbi, and I. Haddouche, *Supercontinnum generation in silica photonic crystal fiber at 1.3μm and 1.65μm wavelength for optical coherence tomography*, Optik **152** (2018), 106–115.
75. M. Sharma, S. Konar, and R. K. Khan, *Supercontinuum generation in highly nonlinear hexagonal photonic crystal fiber at very low power*, J. Nanophoton. **9** (2015), 1–8.
76. G. D. Kirishna et al., *Analysis of zero dispersion shift and supercontinuum generation near IR in circular photonic crystal fibers*, Optik **145** (2017), 599–607.
77. Y. E. Monfared and S. A. Ponomarenko, *Extremely nonlinear carbon-disulfide-filled photonic crystal fiber with controllable dispersion*, Opt. Material. **88** (2019), 406–411.

AUTHOR BIOGRAPHIES

Pranaw Kumar is an Assistant Professor in School of Electronics Engineering, Kalinga Institute of Industrial Technology University, Bhubaneswar, Odisha, India. He received his Master of Technology in Communication Engineering in 2012 from MNIT Jaipur. He is a member of OSA, SPIE, and Life-member of Indian Science Congress Association. He is also an IEEE student member. His research interests include photonic crystal fibers, optical communication, microstrip antenna, communication, and signal processing. He has published approximately 120 papers in international journals and conferences in the aforementioned research areas. He serves as a reviewer for many international journals

Kokou Firmin Fiaboe received his B.Tech in electronics and electrical engineering from Ecole Nationale Supérieure d'Ingenieurs(ENSI) of Université de Lomé, Lomé, Rep. of Togo in 2016 and his M.Tech degree in electronics and telecommunication engineering from Kalinga Institute of Industrial Technology, Bhubaneswar, Odisha, India in 2019. His current research interests include photonic crystal fibers, and supercontinuum generation.

Jibendu Sekhar Roy is a professor in the school of electronics engineering, KIIT University, Bhubaneswar, Odisha, India. Earlier he was a professor in ECE department, BIT, Mesra, Ranchi, India. He received his PhD from ETCE department, Jadavpur University, Calcutta, India and was a post-doctoral research associate of CNRS (Gov. of France) in IRCOM, University of Limoges, France. His research interests include antenna engineering, wave propagation through optical guiding structures, mobile communication, and signal processing. He has published approximately 250 papers in international journals and conferences. He serves as a reviewer for many international journals. He has visited France, USA, Italy, Indonesia, Denmark, Czech Republic, South Korea, Russia for paper presentations, invited talks, and as a session chair. He is a senior associate of ICTP, Trieste, Italy and member of many other technical societies.